

Make Me a BNN: A Simple Strategy for Estimating Bayesian Uncertainty from Pre-trained Models

Gianni Franchi,^{1, *, †} Olivier Laurent,^{1, 2, *} Maxence Leguéry,¹ Andrei Bursuc,³
 Andrea Pilzer⁴ & Angela Yao⁵
 U2IS, ENSTA Paris, Institut Polytechnique de Paris,¹ Université Paris-Saclay,²
 NVIDIA,³ valeo.ai,⁴ National University of Singapore⁵

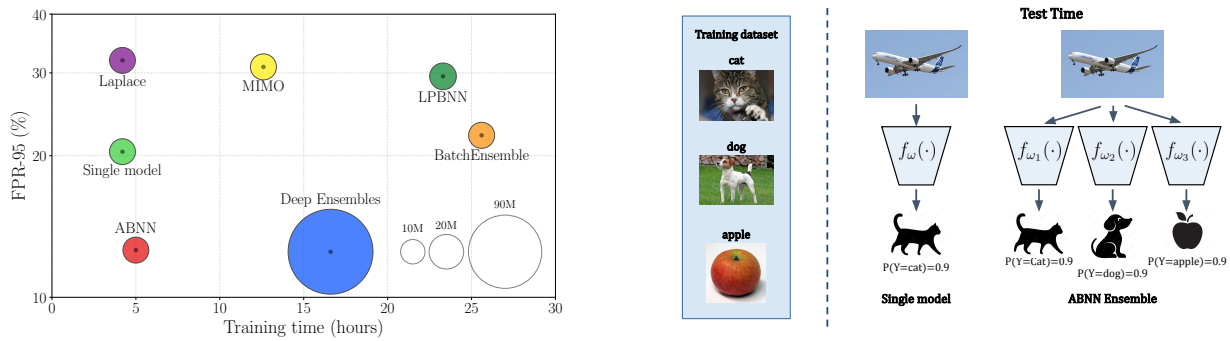


Figure 1. **Benefits of the ABNN approach.** (left) Evaluation of the trade-off between computational cost (training time and model size) and performance (in terms of FPR95 score, lower the better) for various uncertainty quantification techniques on CIFAR-10 [49] with WideResNet [94] and ensembles of size 4. (right) Using ABNN ensembling at test time: given an out-of-distribution input, a simple DNN may make a high-confidence incorrect predictions, whereas ABNN produces more uncertain decisions through its diverse predictions.

Abstract

Deep Neural Networks (DNNs) are powerful tools for various computer vision tasks, yet they often struggle with reliable uncertainty quantification — a critical requirement for real-world applications. Bayesian Neural Networks (BNN) are equipped for uncertainty estimation but cannot scale to large DNNs that are highly unstable to train. To address this challenge, we introduce the Adaptable Bayesian Neural Network (ABNN), a simple and scalable strategy to seamlessly transform DNNs into BNNs in a post-hoc manner with minimal computational and training overheads. ABNN preserves the main predictive properties of DNNs while enhancing their uncertainty quantification abilities through simple BNN adaptation layers (attached to normalization layers) and a few fine-tuning steps on pre-trained models. We conduct extensive experiments across multiple datasets for image classification and semantic segmentation tasks, and our results demonstrate that ABNN achieves state-of-the-art performance without the computational budget typically associated with ensemble methods.

*equal contribution, † gianni.franchi@ensta-paris.fr

1. Introduction

Deep Neural Networks (DNNs) have emerged as powerful tools with a profound impact on various perception tasks, such as image classification [18, 50], object detection [32, 70], natural language processing [17, 69, 76], etc. With this progress, there is growing excitement and expectation about the potential applications of DNNs across industries. To meet this end, there is a critical need to address a fundamental challenge: improving DNN reliability by quantifying the inherent uncertainty in their predictions [36, 37, 82]. Deploying DNNs in real-world applications, particularly in safety-critical domains such as autonomous driving, medical diagnoses, industrial visual inspection, etc., requires a comprehensive understanding of their limitations and vulnerabilities beyond their raw predictive accuracy, often considered a primary performance metric. By quantifying the uncertainty within these models with millions of parameters and non-trivial inner-working [1, 93] and failure modes [33, 66] in front of the many different long-tail scenarios [7, 56], we can make informed decisions about when and how to rely on their predictions.

In deep learning, uncertainty estimation has been tra-

ditionally addressed under Bayesian approaches drawing inspiration from findings in Bayesian Neural Networks (BNNs) [5, 58, 64, 85] that stand on solid theoretical grounds and properties [44, 62, 89]. BNNs estimate the posterior distribution of the model parameters given the training dataset. Ensembles can be sampled from this distribution at runtime, and their predictions can be averaged for reliable decisions. BNNs promise improved predictions and reliable uncertainty estimates with intuitive decomposition of the uncertainty sources [16, 41]. However, although they are easy to formulate, BNNs are notoriously difficult to train over large DNNs [20, 67], in particular for complex computer vision tasks, due to training instability and computational inefficiency as they are typically trained through variational inference [45]. This limitation of BNNs has inspired two major lines of research toward scalable uncertainty estimation: ensembles and last-layer uncertainty approaches.

Deep Ensembles [51] emerge as a simple and highly effective alternative to BNNs for uncertainty estimation on large DNNs. Deep Ensembles are trivial to train by essentially instantiating the same training procedure over different weight initializations of the same network and have been shown to preserve many of the properties of BNNs in terms of predictions diversity [22, 89]. This is a beneficial property for out-of-distribution (OOD) generalization [63]. However, their high computational cost (during both training and inference) makes them inapplicable to many practical applications with computational constraints. In the last few years, multiple computationally efficient alternatives have emerged aiming to reduce training cost during training and inference [13, 23, 25, 26, 30, 59, 86]. However, these methods propose specific network architectures and non-trivial trade-offs in computational cost, accuracy, and predictive uncertainty quality.

Last-layer uncertainty approaches aim for BNNs with fewer stochastic weights to produce ensembles or uncertainty estimates [6, 9, 12, 48, 60]. These methods leverage popular DNN architectures [31] to which they attach a stochastic layer and train all parameters for a complete training cycle. While training stability is improved compared to standard BNNs, joint optimization of deterministic and stochastic parameters requires careful tuning. Daxberger et al. [12] propose training the last layer separately in a *post-hoc* manner effectively leveraging Laplace approximation for optimization [58, 72, 80]. Decoupling the optimization of the encoder from the uncertainty layer enables the use of the typical training recipes for the encoder or simply leveraging off-the-shelf pre-trained networks. The limitation of last-layer methods is related to the access to only high-level features for producing uncertainty estimates. In contrast, signals of distribution shift or small anomaly patterns (e.g., in semantic segmentation) can be found primarily on low-level features earlier in the network.

Indeed, strong uncertainty estimation methods leverage information from multiple layers of the networks [13, 25, 55].

In this work, we aim for scalable and effective uncertainty estimation without sophisticated optimization schemes and potential training instability and without compromising predictive performance. We propose a post-hoc strategy that starts from a pre-trained DNN and transforms it into a BNN with a simple plug-in module attached to the normalization layers and only a few epochs of fine-tuning. We show that this strategy, dubbed Adaptable-BNN (ABNN), can estimate the posterior distribution around the local minimum of the pre-trained model in a resource-efficient manner while still achieving competitive uncertainty estimates with diversity. Furthermore, ABNN allows for sequential training of multiple BNNs starting from the same checkpoint, thus modeling various modes within the true posterior distribution.

Our contributions are: **(1)** We propose ABNN, a simple strategy to transform a pre-trained DNN into a BNN with uncertainty estimation capabilities. ABNN is computationally efficient and compatible with multiple DNN architectures (ConvNets: ResNet-50, WideResnet28-10; ViTs), provided they are equipped with normalization layers. **(2)** We observe that the variance of the gradient for ABNN’s parameters is lower compared to that of a classic BNN, resulting in a more stable backpropagation. **(3)** Extensive experiments validate that ABNN, although simple and computationally frugal, achieves competitive performance in terms of accuracy and uncertainty estimation over multiple datasets and tasks: image classification (CIFAR-10, CIFAR-100 [49], ImageNet [15]) and semantic segmentation (StreetHazards, BDD-Anomaly [35], MUAD [24]) in both in- and out-of-distribution settings.

2. Related work

Epistemic uncertainty and Bayesian posterior. Tackling epistemic uncertainty estimation [39] - the uncertainty on the model itself - is essential to improve the reliability of DNNs [41]. However, obtaining satisfying approximations of this uncertainty remains a challenge as it requires a scalable estimation of the extremely high dimensional distribution of the weights, the *posterior*. Our work presents ABNN, a significantly more scalable method compared to the BNNs [28] that predominantly shape the landscape of epistemic uncertainty estimations [27].

Bayesian Neural Networks and Ensembles. BNNs [81] formulate probabilistic predictions by both introducing explicit and controllable prior knowledge on the network weights [46, 64] and estimating the posterior. While formulating mathematically, the posterior distribution is possible [89], its computation for modern models is intractable. This need for scalability leads to approximation techniques that include variational inference [4, 5] BNNs, which fit

simpler distributions to the posterior (diagonal Gaussian for the former). Many other approximation methods have been proposed, like the efficient probabilistic backpropagation [38], Monte-Carlo Dropout [26] that model the posterior as a mixture of Diracs and Laplace methods that estimate the posterior thanks to the local curvature of the loss [58, 72, 74, 80]. However, *deep ensembles* [29, 51], the most successful solution is simpler. It consists of simply averaging the predictions of several independently trained models. This method is powerful as it improves the reliability and the quality of the predictions, albeit costly in training and inference. Many approximate methods stepped into the breach and proposed to reduce the number of parameters, the training time, or the number of forward passes [23, 25, 30, 54, 86, 90]. The proposed method is in this line of scalability and computational efficiency.

Post-hoc uncertainty quantification. In today’s context of computer vision, with ever-increasing datasets [47, 75], model sizes [14], and inference constraints, post-hoc methods could be a solution to benefit from both the power of foundation models [42, 73, 95] and uncertainty quantification. The Laplace method reigns among these post-hoc uncertainty quantification methods, especially with its last-layer approximations [72] that make them even more scalable. However, even with the coarse approximation of the posterior achieved by Kronecker-factored Laplace [74], it is not always very efficient with modern datasets. We propose a straightforward and effective method that works with pre-trained models.

3. Background

We start by introducing our formalism and a brief overview of the Bayesian posterior and BNNs for uncertainty quantification.

3.1. Preliminaries

Notations. Let us denote $\mathcal{D} = \{(\mathbf{x}_i, y_i)\}_{i=1}^N$ the training set containing N samples and labels drawn from a joint distribution $P_{(X,Y)}$. The input $\mathbf{x}_i \in \mathbb{R}^d$ is processed by a neural network f_ω , of parameters ω , that outputs classification predictions $\hat{y}_i = f_\omega(\mathbf{x}_i) \in \mathbb{R}$.

From MLE to MAP. In our context, $P(Y = y_i | X = \mathbf{x}_i, \omega)$ is a categorical distribution over the classes within the range of Y . We omit the random variable notation in the following for clarity. The log-likelihood of this distribution typically corresponds to the cross-entropy loss, which practitioners often minimize with stochastic gradient descent to obtain a maximum likelihood estimate (MLE): $\mathcal{L}_{\text{MLE}}(\omega) = -\sum_{(\mathbf{x}_i, y_i) \in \mathcal{D}} \log P(y_i | \mathbf{x}_i, \omega)$.

Going further, the Bayesian framework allows us to incorporate prior knowledge regarding ω denoted as the distribution $P(\omega)$ that complements the likelihood and leads to the research of the maximum a posteriori (MAP), via the

minimization of the following loss function:

$$\mathcal{L}_{\text{MAP}}(\omega) = -\sum_{(\mathbf{x}_i, y_i) \in \mathcal{D}} \log P(y_i | \mathbf{x}_i, \omega) - \log P(\omega). \quad (1)$$

The normal prior is the standard choice for $P(\omega)$, leading to the omnipresent L2 weight regularization.

3.2. Bayesian Posterior and BNNs

Typically, DNNs retain a single set of weights ω_{MAP} at the end of the training to use at inference. As such, we de facto consider this model as an oracle. In contrast, BNNs attempt to model the posterior distribution $P(\omega | \mathcal{D})$ to take all possible models into account. The prediction y for a new sample \mathbf{x} is computed as the expected outcome from an infinite ensemble, including all possible weights sampled from the posterior distribution:

$$P(y | \mathbf{x}, \mathcal{D}) = \int_{\omega \in \Omega} P(y | \mathbf{x}, \omega) P(\omega | \mathcal{D}) d\omega. \quad (2)$$

However, in practice, this Bayes ensemble approach is intractable since the integral Eq. (2) is computed over the entire parameter space Ω . Practitioners [51] approximate this integral by averaging predictions derived from a finite set $\{\omega_1, \dots, \omega_M\}$ of M weight configurations sampled from the posterior distribution:

$$P(y | \mathbf{x}, \mathcal{D}) \approx \frac{1}{M} \sum_{m=1}^M P(y | \mathbf{x}, \omega_m). \quad (3)$$

Let us start with a simple Multi-Layer Perceptron (MLP) with two hidden layers without loss of generality. For a given input data point \mathbf{x} , the prediction of the DNN is defined as, with \mathbf{h}_1 and \mathbf{h}_2 the preactivation maps, $a(\cdot)$ the activation function:

$$\begin{aligned} \mathbf{h}_1 &= W^{(1)} \mathbf{x} \\ \mathbf{u}_1 &= \text{norm}(\mathbf{h}_1, \beta_1, \gamma_1) = \frac{\mathbf{h}_1 - \hat{\mu}_1}{\hat{\sigma}_1} \times \gamma_1 + \beta_1 \\ \mathbf{a}_1 &= a(\mathbf{u}_1) \\ \mathbf{u}_2 &= \text{norm}\left(W^{(2)} \mathbf{a}_1, \beta_2, \gamma_2\right), \text{ and } \mathbf{a}_2 = a(\mathbf{u}_2) \\ \mathbf{h}_3 &= W^{(3)} \mathbf{a}_2, \text{ and } P(y | \mathbf{x}, \omega) = \text{soft}(\mathbf{h}_3) \end{aligned} \quad (4)$$

In Eq. (4), $\text{soft}(\cdot)$ is the softmax, \mathbf{a}_1 and \mathbf{a}_2 are the hidden activations, and $\{W^{(j)}\}_{j \in \{0,1,2\}}$ correspond to the weights of the linear layers. The operator $\text{norm}(\cdot, \beta_j, \gamma_j)$, of trainable parameters β_j and γ_j , can refer to any batch, layer, or instance normalization (BN, LN, IN). Finally, norm comes with its empirical mean $\hat{\mu}_{\mathbf{u}_j}$ and variance $\hat{\sigma}_{\mathbf{u}_j}$. We omit the small value often added for computational stability.

In the current form, we can leverage this architecture to learn different tasks. However, modeling the uncertainty of

the predictions beyond the use of softmax scores as confidence proxies is non-trivial. BNNs [5] are one solution to improve uncertainty estimation. Generally, they hypothesize the independence of the layers and sample from the resulting posterior estimate. For the j -th layer, this yields:

$$\begin{aligned} \mathbf{u}_j &= \text{norm}(W^{(j)}\mathbf{x}, \beta_j, \gamma_j), W^{(j)} \sim P(W^{(j)}|\mathcal{D}), \text{ and} \\ \mathbf{a}_j &= a(\mathbf{u}_j). \end{aligned} \quad (5)$$

As such, BNNs approximate the marginalization (2) of the parameters - an extremely complex task - by generating multiple predictions. Variational inference BNNs [5], the most scalable version among these methods, base their estimation on the "reparametrization trick", here at layer j :

$$\begin{aligned} \mathbf{u}_j &= \text{norm} \left(\left[W_\mu^{(j)} + \epsilon_j W_\sigma^{(j)} \right] \mathbf{h}_{j-1}, \beta_j, \gamma_j \right) \text{ and} \\ \mathbf{a}_j &= a(\mathbf{u}_j), \end{aligned} \quad (6)$$

where the matrices $W_\mu^{(j)}$ and $W_\sigma^{(j)}$ denote the mean and standard deviation of the posterior distribution of layer j , and $\epsilon_j \sim \mathcal{N}(\mathbf{0}, \mathbf{1})$ is a zero-mean unit-diagonal Gaussian vector or matrix. This method enables learning an estimate of a diagonal posterior distribution at the cost of tripling the number of parameters compared to a standard network.

4. ABNN

4.1. Converting DNNs into BNNs

We base our post-hoc Bayesian strategy on pre-trained DNNs that incorporate normalization layers such as batch [43], layer [3], or instance normalization [83]. This is not a limiting factor as most modern architectures include one type of these layers [18, 31, 57]. Subsequently, we modify these normalization layers by introducing a Gaussian perturbation, incorporating our novel Bayesian Normalization Layer (BNL). This adaptation aims to transform the initially deterministic DNN into a BNN. The introduction of the BNL allows us to efficiently leverage pre-trained models, facilitating the conversion to a BNN with minimal alterations. We propose replacing the normalization layers with our novel Bayesian normalization layers (BNL) that incorporate Gaussian noise to transform the deterministic DNNs into BNNs easily. BNLs unlock the power of pre-trained models for uncertainty-aware Bayesian networks. Formally, our BNN is defined as:

$$\begin{aligned} \mathbf{u}_j &= \mathbf{BNL} \left(W^{(j)}\mathbf{h}_{j-1} \right), \text{ and} \\ \mathbf{a}_j &= a(\mathbf{u}_j) \text{ with} \\ \mathbf{BNL}(\mathbf{h}_j) &= \frac{\mathbf{h}_j - \hat{\mu}_j}{\hat{\sigma}_j} \times \gamma_j(1 + \epsilon_j) + \beta_j. \end{aligned} \quad (7)$$

The empirical mean and variance are still represented by $\hat{\mu}_{\mathbf{u}_j}$ and $\hat{\sigma}_{\mathbf{u}_j}$ and computed through batch, layer or instance normalization. In the equation, $\epsilon_j \sim \mathcal{N}(\mathbf{0}, \mathbf{1})$ signifies a sample drawn from a Normal distribution, and γ_j and β_j are the two learnable vectors of the j -th layer.

The DNN being transformed into a BNN, we exclusively retrain the parameters γ_j and β_j for a limited number of epochs using the loss introduced in Section 4.2. To further improve its reliability and generalization properties [89], we do not train a singular ABNN, but rather multiple copies of ABNNs, as explained in section 4.2, resulting in a finite set $\omega_1, \dots, \omega_M$ of M weight configurations. We discuss the benefits of this multi-modality in Appendix A.2.

During inference, for each sample from ABNN ω_m , we augment the number of samples by independently sampling multiple $\epsilon_j \sim \mathcal{N}(\mathbf{0}, \mathbf{1})$. With ϵ the concatenation of all ϵ_j , and $\{\epsilon_l\}_{l \in [1, L]}$ the set of ϵ s, each individual ABNN sample is expressed as $P(y | x, \omega, \epsilon)$. During inference, the prediction y for a new sample \mathbf{x} is computed as the expected outcome from a finite ensemble, encompassing all the weights sampled from the posterior distribution:

$$P(y | \mathbf{x}, \mathcal{D}) \approx \frac{1}{ML} \sum_{l=1}^L \sum_{m=1}^M P(y | \mathbf{x}, \omega_m, \epsilon_l). \quad (8)$$

4.2. ABNN training loss

The multimodality [22, 44, 53] of the posterior distribution of DNNs is a challenge to any attempt to perform variational inference with on a mono-modal distribution. Wilson and Izmailov [89] have proposed to tackle this issue by training multiple BNNs. However, such approaches inherit the instability of classical BNNs and may struggle to capture different modes accurately. ABNN encounters a similar challenge, requiring safeguards against collapsing into the same local minima during post-training. To mitigate this problem, we introduce a small perturbation to the loss function, preventing collapse and encouraging diversity into the training process. This perturbation involves a modification of the class weights within the cross-entropy loss, now defined as:

$$\mathcal{E}(\omega) = - \sum_{(\mathbf{x}_i, y_i) \in \mathcal{D}} \eta_i \log P(y_i | \mathbf{x}_i, \omega). \quad (9)$$

In this formula, η_i represents the class-dependent random weight we initialize at the beginning of training. Typically, it can be set to zero or one to amplify the effect of certain classes. In contrast to classical variational BNNs [5] that optimize the evidence lower-bound loss, ABNN maximizes the MAP. The optimization involves the following loss:

$$\mathcal{L}(\omega) = \mathcal{L}_{\text{MAP}}(\omega) + \mathcal{E}(\omega). \quad (10)$$

We employ this procedure to train various ABNNs, resulting in ABNNs trained with different losses due to the presence of $\mathcal{E}(\omega)$.

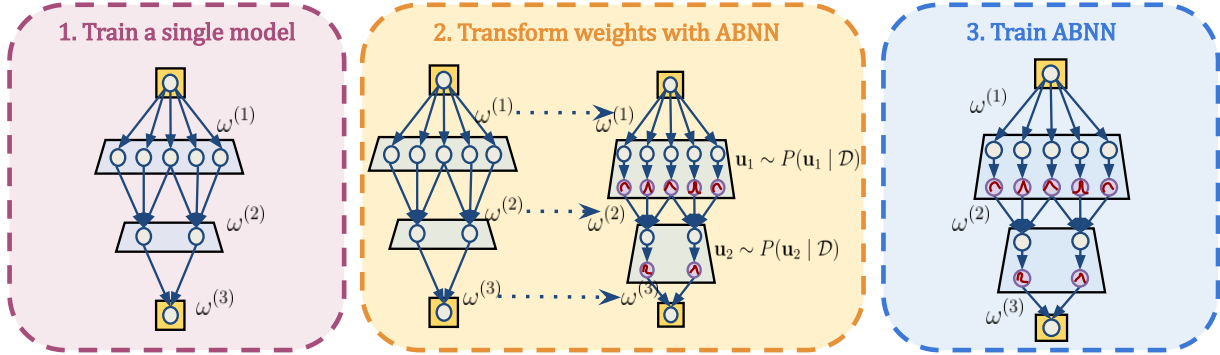


Figure 2. **Illustration of the training process for the ABNN.** The procedure begins with training a single DNN ω_{MAP} , followed by architectural adjustments to transform it into an ABNN. The final step involves fine-tuning the ABNN model.

4.3. ABNN training procedure

ABNN is trained through a post-hoc process designed to leverage the strength of Bayesian concepts and improve the uncertainty prediction of DNNs. The training pseudo code for ABNN, detailed in Alg. 1, outlines the step-by-step process of transforming a conventional DNN into an ensemble of Bayesian models.

We start from a pre-trained neural network (Alg. 1, line 1) and introduce the Bayesian normalization layers, replacing the old batch, instance or layer normalization of the former DNN (Alg. 1 lines 2 to 10). This operation transforms the conventional deterministic network into a BNN to help quantify the uncertainty. We initialize the weights of the new layer with the values of the replaced normalizations.

Then, we fine-tune the modified network to capture better the inherent uncertainty (Alg. 1 lines 12 to 24). The full process is described in Figure 4, providing a clear overview of the modifications made to enable Bayesian modeling. More precisely, we only fine-tune the normalization weights in Table 1. To improve the posterior estimation of our ABNN models, we fine-tune multiple instances of the normalization layers (typically 3 to 4). This ensemble approach provides robustness and contributes to a more reliable estimation of the posterior distribution. Training multiple ABNNs, each starting from the same checkpoint, enhances our ability to capture diverse modes of the true posterior, thereby improving the overall uncertainty quantification.

4.4. Theoretical analysis

Our approach raises several theoretical questions. In the supplementary material - as detailed in Section A.1 - we show that ABNN exhibits greater stability than classical BNNs. Indeed, in variational inference BNNs, the gradients vary greatly: ϵ , crucial for obtaining the Bayesian interpretation, often introduces instability, perturbing the training. ABNN reduces this burden by applying this term on the latent space rather than the weights, thereby reducing the

Algorithm 1 ABNN training procedure

```

1:  $f_{\omega_{\text{MAP}}}$ , : pre-trained network,  $\lambda$  : learning rate,
   nb_epoch : number of epoch
2: (Step 2: adapt the DNN to a DNN)
3: # Build a list of all the normalisation layers
4: normalisation=[Batch_normalisation, Layer_normalisation,
   Instance_normalisation]
5: for layer  $\in$   $f_{\omega_{\text{MAP}}}$ .layers : to do
6:   begin
7:   (Transform all Normalization Layers)
8:   if (layer  $\in$  normalisation) : then
9:     replace layer by BNL
10:  end
11: (Step 3: train ABNN)
12: t=0
13: for (epoch)  $\in$  nb_epoch : to do
14:  begin
15:  for (x, y)  $\in$  trainloader : to do
16:    begin
17:    (Forward pass)
18:     $\forall x_i \in B(t)$  calculate  $f_{\omega^{(t)}}(x_i)$ 
19:    evaluate the loss  $\mathcal{L}(\omega^{(t)}, B(t))$ 
20:     $\omega^{(t)} \leftarrow \omega^{(t-1)} - \lambda \nabla \mathcal{L}_{\omega^{(t)}}$ 
21:    (Step update)
22:     $t \leftarrow t + 1$ 
23:  end
24:  end

```

variance of the gradients, as empirically demonstrated in Appendix A.1.

Another question concerns the theoretical need to modify the loss and add the second term \mathcal{E} . We show in Appendix A.2 that it is theoretically sound in the case of a convex problem. Given that DNN optimization is inherently non-convex, adding this term may be theoretically debatable. However, a sensitivity analysis of this term - developed in Appendix D - shows empirical benefits for performance and uncertainty quantification

Finally, we discuss the challenge of estimating the equiv-

alent BNNs to our networks in Appendix A.3. Despite the theoretical value this information could provide concerning the posterior, it remains unused in practice. We solely sample the ϵ and average over multiple training terms to generate robust predictions during inference.

5. Experiments & Results

We test ABNN on image classification and semantic segmentation tasks. In each case, we measure metrics relative to the performance of the models but measure their uncertainty quantification abilities. All our models are implemented in PyTorch and trained on a single Nvidia RTX 3090. Appendix G details the hyper-parameters used in our experiments across architectures and datasets.

5.1. Image classification

Datasets. We demonstrate the efficiency of ABNN on different datasets and backbones. We start with CIFAR-10 and CIFAR-100 [49] with ResNet-50 [31] and WideResNet28-10 [94]. We then report results for ABNN on ImageNet [15] with ResNet-50 and ViT [18]. In the former case, we train all models from scratch. In the latter, we start from torchviz pre-trained models [68].

Baselines. We compare ABNN against Deep Ensembles [51] and four other ensembles: BatchEnsemble [86], MIMO [30], Masksembles [19], and Laplace [12].

Metrics. We evaluate the performance on classification tasks with the accuracy (Acc) and the Negative Log-Likelihood (NLL). We complete these metrics with the expected top-label calibration error (ECE) [61] and measure the quality of the OOD detection using the Areas Under the Precision/Recall curve (AUPR) and the operating Curve (AUC), as well as the False Positive Rate at 95% recall (FPR95) similarly to Hendrycks et al. [34]. We express all metrics in %.

OOD detection datasets. For OOD detection tasks on CIFAR-10 and CIFAR-100, we use the SVHN dataset [65] as the out-of-distribution dataset and transform the initial problem into binary classification between in-distribution and out-of-distribution data using the maximum softmax probability as the criterion. For ImageNet, we use Describable Texture [84] as the out-of-distribution dataset.

Results. Tables 1 and 2 present the performance of ABNN across various architectures for CIFAR-10/100 and ImageNet, respectively. Notably, ABNN consistently surpasses Laplace approximation and single-model baselines on most datasets and architectures. Furthermore, ABNN exhibits competitive performance compared to Deep Ensembles, achieving equivalent results with a similar number of parameters and training time to a single model. These findings underscore ABNN as a powerful and efficient method, demonstrating superior uncertainty quantification capabilities in image classification tasks while being easier to train.

5.2. Semantic segmentation

For the semantic segmentation part, we compare ABNN against MCP [34], Deep Ensembles [51], MC Dropout [26], TRADI [23], MIMO [30] and LP-BNN [25], on StreetHazards [35], BDD-Anomaly [35], and MUAD [24] that allows comparison on diverse uncertainty quantification aspects of semantic segmentation.

StreetHazards [35]. StreetHazards is a large-scale synthetic dataset comprising various images depicting street scenes. The dataset consists of 5,125 images for training and an additional 1,500 images for testing. The training dataset has pixel-wise annotations available for 13 different classes. The test dataset is designed with 13 classes seen during training and an additional 250 out-of-distribution (OOD) classes that were not part of the training set. This diverse composition allows for assessing the algorithm’s robustness in the face of various potential scenarios. In our experiments, we employed DeepLabv3+ with a ResNet-50 encoder, as introduced by Chen et al. [8].

BDD-Anomaly [35]. BDD-Anomaly, a subset of the BDD100K dataset [91], comprises 6,688 street scenes for training and an additional 361 for the test set. Within the training set, pixel-level annotations are available for 17 distinct classes. The test dataset consists of the same 17 classes seen during training and introduces 2 out-of-distribution (OOD) classes: motorcycle and train. In our experimental setup, we adopted DeepLabv3+[8] and followed the experimental protocol outlined in [35]. Similar to previous experiments, we utilized a ResNet-50 encoder [31] for the neural network architecture.

MUAD [24]. MUAD consists of 3,420 images in the training set and 492 in the validation set. The test set comprises 6,501 images, distributed across various subsets: 551 in the normal set, 102 in the normal set with no shadow, 1,668 in the out-of-distribution (OOD) set. All these sets cover both day and night conditions, with a distribution of 2/3 day images and 1/3 night images. MUAD encompasses 21 classes, with the initial 19 classes mirroring those found in CityScapes [10]. Additionally, three classes are introduced to represent object anomalies and animals, adding diversity to the dataset. In our first experiment, we employed a DeepLabV3+ [8] network with a ResNet50 encoder [31] for training on MUAD.

Results. Table 3 presents the results of ABNN, compared to various baselines on the three datasets. ABNN performs competitively with Deep Ensembles, a technique known for accurately quantifying uncertainty. Moreover, our approach exhibits faster training times, making it potentially more appealing for practitioners. We have not included a comparison with Laplace Approximation, as it is not commonly applied to semantic segmentation, and adapting DNNs for Laplace Approximation is not straightforward.

		Method	Acc \uparrow	NLL \downarrow	ECE \downarrow	AUPR \uparrow	AUC \uparrow	FPR95 \downarrow	Δ Param \downarrow	Time (h) \downarrow
CIFAR-10	ResNet-50	Single Model	95.1	0.211	3.1	95.2	91.9	23.6	\emptyset	1.7
		BatchEnsemble	93.9	0.255	3.3	94.7	91.3	20.1	0.11	17.2
		MIMO ($\rho = 1$)	95.4	0.197	3.0	95.1	90.8	26.0	0.07	6.7
		LPBNN	95.0	0.251	9.4	98.4	96.9	10.3	1.83	17.2
		Deep Ensembles	96.0	0.136	0.8	97.0	94.7	15.5	70.56	6.8
		Laplace	95.3	0.160	1.3	96.0	93.3	18.8	/	1.7
		ABNN	95.4	0.215	0.845	97.0	94.7	15.1	0.16	2.0
	WideResNet-28 \times 10	Single Model	95.4	0.200	2.9	96.1	93.2	20.4	\emptyset	4.2
		BatchEnsemble	95.6	0.206	2.7	95.5	92.5	22.1	0.10	25.6
		MIMO ($\rho = 1$)	94.7	0.234	3.4	94.9	90.6	30.9	0.12	12.6
		LPBNN	95.1	0.249	2.9	95.4	91.2	29.5	0.71	23.3
		Deep Ensembles	95.8	0.143	1.3	97.8	96.0	12.5	109.47	16.6
		Laplace	95.6	0.151	0.8	95.0	90.7	31.9	/	4.2
		ABNN	93.7	0.198	1.8	98.5	96.9	12.6	0.05	5.0
CIFAR-100	ResNet-50	Single Model	78.3	0.905	8.9	87.4	77.9	57.6	\emptyset	1.7
		BatchEnsemble	66.6	1.788	18.2	85.2	74.6	60.6	0.11	17.2
		MIMO ($\rho = 1$)	79.0	0.876	7.9	87.5	76.9	64.7	0.63	6.7
		LPBNN	78.5	1.02	11.3	88.2	77.8	73.5	1.83	17.2
		Deep Ensembles	80.9	0.713	2.6	89.2	80.8	52.5	71.12	6.8
		Laplace	78.2	0.987	14.2	89.2	81.0	51.8	/	1.7
		ABNN	78.9	0.889	5.5	89.4	81.0	50.1	0.16	2.0
	WideResNet-28 \times 10	Single Model	80.3	0.963	15.6	81.0	64.2	80.1	\emptyset	4.2
		BatchEnsemble	82.3	0.835	13.0	88.1	78.2	69.8	0.10	25.6
		MIMO ($\rho = 1$)	80.2	0.822	2.8	84.9	72.0	72.8	0.19	12.6
		LPBNN	79.7	0.831	7.0	79.0	70.1	71.4	0.72	23.3
		Deep Ensembles	82.5	0.903	22.9	81.6	67.9	71.3	109.64	16.6
		Laplace	80.1	0.942	16.0	83.4	72.1	59.9	/	4.2
		ABNN	80.4	1.08	5.5	85.0	75.0	57.7	0.05	5.0

Table 1. **Performance comparison (averaged over five runs) on CIFAR-10/100 using ResNet-50 and Wide ResNet28 \times 10.** All ensembles have $M = 4$ subnetworks. we highlight the best performances in bold. The ResNet-50 single model has respectively $\{23.52, 23.70\} \cdot 10^6$ parameters. Δ Param is the number of parameters in excess of the corresponding method compared to the single model. Time is the training time in hours on a single RTX 3090.

		Method	Acc \uparrow	ECE \downarrow	AUPR \uparrow	AUC \uparrow	FPR95 \downarrow
ResNet-50	Single Model	77.8	12.1	18.0	80.9	68.6	
	BatchEnsemble	75.9	3.5	20.2	81.6	66.5	
	MIMO ($\rho = 1$)	77.6	14.7	18.4	81.6	66.8	
	Deep Ensembles	79.2	23.3	19.6	83.4	62.1	
	Laplace	80.4	44.3	13.9	75.9	82.8	
	ABNN	79.5	9.65	17.8	82.0	65.2	
ViT	Single Model	80.0	5.2	19.5	84.1	58.5	
	Deep Ensembles	81.7	13.5	21.7	85.5	60.3	
	Laplace	81.0	10.8	22.1	83.1	70.6	
	ABNN	80.6	4.32	21.7	85.4	55.1	

Table 2. **Performance on ImageNet using ResNet-50 and ViT** concerning in distribution and out-of-distribution metrics.

6. Discussions

6.1. General discussions

We develop several discussions in the supplementary materials. First, we explore the theoretical aspects, including the stability of the DNNs in Appendix A.1, the importance of multi-mode in Section A.2, and the relationship with classical BNNs in Appendix A.3. We experiment on the transfer of ViT-B-16 from Imagenet 21k [71] to CIFAR-100

which highlights the potential of ABNN in transfer learning, achieving an accuracy of 92.18%. Additionally, we perform several ablation studies, notably on the impact of discarding multi-mode or the loss term \mathcal{E} (defined in Section 4.2) in Appendix D. We show that discarding \mathcal{E} reduces the performance while incorporating the multi-mode improves uncertainty quantification. Moreover, in Section B, we analyze the variance of the gradients, confirming that our technique exhibits lower gradients than BNNs, making it more stable and easier to train. Finally, Appendix C delves into the variability of our method under different scenarios, exploring cases where we initiate ABNN from a single model and optimize from various initial checkpoints. Although our technique inherits the instabilities of the DNN, we observe that the standard variation is five times larger than that of the single model, indicating less stability than a standard DNN.

6.2. Diversity of ABNN

Concerning the diversity, we train ABNN on CIFAR-10 using a ResNet-50 architecture. Specifically, we optimize a ResNet for 200 epochs and then fine-tune three ABNNs, starting from the optimal checkpoint. Additionally, we train two other ResNet-50s on CIFAR-10 to form a proper Deep

	Method	mIoU \uparrow	AUPR \uparrow	AUC \uparrow	FPR95 \downarrow	ECE \downarrow
StreetHazards	Single Model	53.90	6.91	86.60	35.74	6.52
	TRADI	52.46	6.93	87.39	38.26	6.33
	Deep Ensembles	55.59	8.32	87.94	30.29	5.33
	MIMO	55.44	6.90	87.38	32.66	5.57
	BatchEnsemble	56.16	7.59	88.17	32.85	6.09
	LP-BNN	54.50	7.18	88.33	32.61	5.20
	ABNN (ours)	53.82	7.85	88.39	32.02	6.09
BDD-Anomaly	Single Model	47.63	4.50	85.15	28.78	17.68
	TRADI	44.26	4.54	84.80	36.87	16.61
	Deep Ensembles	51.07	5.24	84.80	28.55	14.19
	MIMO	47.20	4.32	84.38	35.24	16.33
	BatchEnsemble	48.09	4.49	84.27	30.17	16.90
	LP-BNN	49.01	4.52	85.32	29.47	17.16
	ABNN (ours)	48.76	5.98	85.74	29.01	14.03
MUAD	Single Model	57.32	26.04	86.24	39.43	6.07
	MC-Dropout	55.62	22.25	84.39	45.75	6.45
	Deep Ensembles	58.29	28.02	87.10	37.60	5.88
	BatchEnsemble	57.10	25.70	86.90	38.81	6.01
	MIMO	57.10	24.18	86.62	34.80	5.81
	ABNN (ours)	61.96	24.37	91.55	21.68	5.58

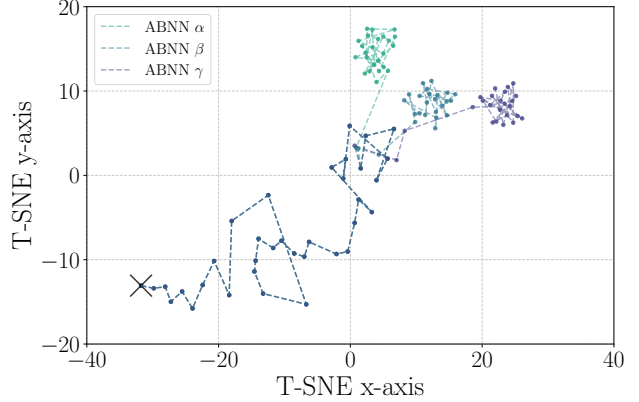
Table 3. **Comparative results on the OOD task for semantic segmentation.** We run all methods in similar settings using publicly available code for related methods. Results are averaged over three seeds. The architecture is a DeepLabv3+ based on ResNet50.

Ensembles. As depicted in Figure 3, ABNN does not exhibit the same level of diversity as the Deep Ensembles. However, it is intriguing that even when initiated from a single DNN, ABNN manages to depart from its local minimum and explore different modes. This concept of different modes is further supported by Section E, where we analyze the mutual information of various ABNN checkpoints.

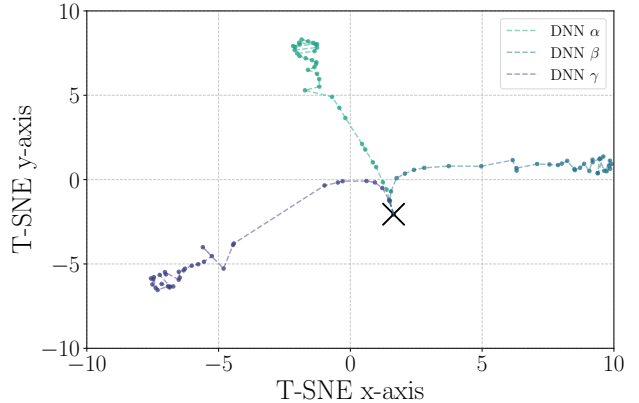
7. Conclusion

In conclusion, our proposed approach, ABNN, introduces a novel perspective to uncertainty quantification. Leveraging the strengths of pre-trained deterministic models, ABNN strategically transforms them into Bayesian networks with minimal modifications, offering enhanced stability and efficient posterior exploration. Through comprehensive experimental analyses, we demonstrate the effectiveness of ABNN both in predictive performance and uncertainty quantification, showcasing its potential applications in diverse scenarios.

The multi-mode characteristic of ABNN, coupled with a carefully designed loss function, not only addresses the challenge of the multi-modality of the posterior but also provides a stable and diverse ensemble of models. Our empirical evaluations on various datasets and architectures highlight the superiority of ABNN over traditional BNNs and post-hoc uncertainty quantification methods such as the Laplace approximation and showcase its competitiveness compared to state-of-the-art such as Deep Ensembles.



(a) ABNN



(b) Deep Ensembles

Figure 3. **Comparison of the diversities of ABNN and Deep Ensembles [51].** T-SNE plot of the 20 principal components of the logits generated from 384 images for ABNN (a) and Deep Ensembles (b).

Moreover, ABNN exhibits promising results in transfer learning scenarios, underscoring its versatility and potential for broader applications. The insights gained from theoretical discussions and ablation studies further elucidate the underlying mechanisms of ABNN, contributing to a deeper understanding of its behavior and performance.

In summary, ABNN emerges as a robust and flexible solution for uncertainty-aware deep learning, offering a pragmatic bridge between deterministic and Bayesian paradigms. Its simplicity in implementation, coupled with superior performance and stability, positions ABNN as a valuable tool in the contemporary landscape of machine learning and Bayesian modeling.

Acknowledgments

This work was performed using HPC resources from GENCI-IDRIS (Grant 2022 - AD011011970R2) and (Grant 2023 - Grant 2022 - AD011011970R3).

References

- [1] Alejandro Barredo Arrieta, Natalia Díaz-Rodríguez, Javier Del Ser, Adrien Bénéttot, Siham Tabik, Alberto Barbado, Salvador García, Sergio Gil-López, Daniel Molina, Richard Benjamins, et al. Explainable artificial intelligence (xai): Concepts, taxonomies, opportunities and challenges toward responsible ai. *Information fusion*, 2020. 1
- [2] Arsenii Ashukha, Alexander Lyzhov, Dmitry Molchanov, and Dmitry Vetrov. Pitfalls of in-domain uncertainty estimation and ensembling in deep learning. In *ICLR*, 2019. 17
- [3] Jimmy Lei Ba, Jamie Ryan Kiros, and Geoffrey E Hinton. Layer normalization. In *NeurIPS*, 2016. 4
- [4] David M Blei, Alp Kucukelbir, and Jon D McAuliffe. Variational inference: A review for statisticians. *JASA*, 2017. 2
- [5] Charles Blundell, Julien Cornebise, Koray Kavukcuoglu, and Daan Wierstra. Weight uncertainty in neural network. In *ICML*, 2015. 2, 4, 13
- [6] Nicolas Brosse, Carlos Riquelme, Alice Martin, Sylvain Gelly, and Éric Moulines. On last-layer algorithms for classification: Decoupling representation from uncertainty estimation. *arXiv preprint arXiv:2001.08049*, 2020. 2
- [7] Robin Chan, Krzysztof Lis, Svenja Uhlemeyer, Hermann Blum, Sina Honari, Roland Siegwart, Pascal Fua, Mathieu Salzmann, and Matthias Rottmann. Segmentmeifyoucan: A benchmark for anomaly segmentation. In *NeurIPS*, 2021. 1
- [8] Liang-Chieh Chen, Yukun Zhu, George Papandreou, Florian Schroff, and Hartwig Adam. Encoder-decoder with atrous separable convolution for semantic image segmentation. In *ECCV*, 2018. 6
- [9] Charles Corbière, Marc Lafon, Nicolas Thome, Matthieu Cord, and Patrick Pérez. Beyond first-order uncertainty estimation with evidential models for open-world recognition. In *ICMLW*, 2021. 2
- [10] Marius Cordts, Mohamed Omran, Sebastian Ramos, Timo Rehfeld, Markus Enzweiler, Rodrigo Benenson, Uwe Franke, Stefan Roth, and Bernt Schiele. The cityscapes dataset for semantic urban scene understanding. In *CVPR*, 2016. 6
- [11] Ekin D Cubuk, Barret Zoph, Jonathon Shlens, and Quoc V Le. Randaugment: Practical automated data augmentation with a reduced search space. In *CVPR*, 2020. 18
- [12] Erik Daxberger, Agustinus Kristiadi, Alexander Immer, Runa Eschenhagen, Matthias Bauer, and Philipp Hennig. Laplace redux—effortless Bayesian deep learning. In *NeurIPS*, 2021. 2, 6
- [13] Erik Daxberger, Eric Nalisnick, James U Allingham, Javier Antorán, and José Miguel Hernández-Lobato. Bayesian deep learning via subnetwork inference. In *ICML*, 2021. 2
- [14] Mostafa Dehghani, Josip Djolonga, Basil Mustafa, Piotr Padlewski, Jonathan Heck, Justin Gilmer, Andreas Peter Steiner, Mathilde Caron, Robert Geirhos, Ibrahim Alabdulmohsin, et al. Scaling vision transformers to 22 billion parameters. In *ICML*, 2023. 3
- [15] Jia Deng, Wei Dong, Richard Socher, Li-Jia Li, Kai Li, and Li Fei-Fei. Imagenet: A large-scale hierarchical image database. In *CVPR*, 2009. 2, 6
- [16] Stefan Depeweg, Jose-Miguel Hernandez-Lobato, Finale Doshi-Velez, and Steffen Udluft. Decomposition of uncertainty in bayesian deep learning for efficient and risk-sensitive learning. In *ICML*, 2018. 2
- [17] Jacob Devlin, Ming-Wei Chang, Kenton Lee, and Kristina Toutanova. Bert: Pre-training of deep bidirectional transformers for language understanding. *arXiv preprint arXiv:1810.04805*, 2018. 1
- [18] Alexey Dosovitskiy, Lucas Beyer, Alexander Kolesnikov, Dirk Weissenborn, Xiaohua Zhai, Thomas Unterthiner, Mostafa Dehghani, Matthias Minderer, Georg Heigold, Sylvain Gelly, et al. An image is worth 16x16 words: Transformers for image recognition at scale. In *ICLR*, 2021. 1, 4, 6
- [19] Nikita Durasov, Timur Bagautdinov, Pierre Baque, and Pascal Fua. Masksembles for uncertainty estimation. In *CVPR*, 2021. 6
- [20] Michael Dusenberry, Ghassen Jerfel, Yeming Wen, Yian Ma, Jasper Snoek, Katherine Heller, Balaji Lakshminarayanan, and Dustin Tran. Efficient and scalable bayesian neural nets with rank-1 factors. In *ICML*, 2020. 2, 13, 15
- [21] William Feller. *An introduction to probability theory and its applications, Volume 2*. John Wiley & Sons, 1991. 15
- [22] Stanislav Fort, Huiyi Hu, and Balaji Lakshminarayanan. Deep ensembles: A loss landscape perspective. *arXiv preprint arXiv:1912.02757*, 2019. 2, 4, 17
- [23] Gianni Franchi, Andrei Bursuc, Emanuel Aldea, Séverine Dubuisson, and Isabelle Bloch. Tradi: Tracking deep neural network weight distributions. In *ECCV*, 2020. 2, 3, 6
- [24] Gianni Franchi, Xuanlong Yu, Andrei Bursuc, Angel Tena, Rémi Kazmierczak, Séverine Dubuisson, Emanuel Aldea, and David Filliat. Muad: Multiple uncertainties for autonomous driving, a benchmark for multiple uncertainty types and tasks. In *BMVC*, 2022. 2, 6
- [25] Gianni Franchi, Andrei Bursuc, Emanuel Aldea, Séverine Dubuisson, and Isabelle Bloch. Encoding the latent posterior of bayesian neural networks for uncertainty quantification. *T-PAMI*, 2023. 2, 3, 6
- [26] Yarin Gal and Zoubin Ghahramani. Dropout as a bayesian approximation: Representing model uncertainty in deep learning. In *ICML*, 2016. 2, 3, 6
- [27] Jakob Gawlikowski, Cedric Robile Njietcheu Tassi, Mohsin Ali, Jongseok Lee, Matthias Humt, Jianxiang Feng, Anna Kruspe, Rudolph Triebel, Peter Jung, Ribana Roscher, et al. A survey of uncertainty in deep neural networks. *Artificial Intelligence Review*, 2023. 2
- [28] Ethan Goan and Clinton Fookes. Bayesian neural networks: An introduction and survey. *Case Studies in Applied Bayesian Data Science*, 2020. 2
- [29] Lars Kai Hansen and Peter Salamon. Neural network ensembles. *IEEE transactions on pattern analysis and machine intelligence*, 1990. 3
- [30] Marton Havasi, Rodolphe Jenatton, Stanislav Fort, Jeremiah Zhe Liu, Jasper Snoek, Balaji Lakshminarayanan, Andrew Mingbo Dai, and Dustin Tran. Training independent subnetworks for robust prediction. In *ICLR*, 2021. 2, 3, 6

- [31] Kaiming He, Xiangyu Zhang, Shaoqing Ren, and Jian Sun. Deep residual learning for image recognition. In *CVPR*, 2016. 2, 4, 6
- [32] Kaiming He, Georgia Gkioxari, Piotr Dollár, and Ross Girshick. Mask r-cnn. In *ICCV*, 2017. 1
- [33] Matthias Hein, Maksym Andriushchenko, and Julian Bitterwolf. Why relu networks yield high-confidence predictions far away from the training data and how to mitigate the problem. In *CVPR*, 2019. 1
- [34] Dan Hendrycks and Kevin Gimpel. A baseline for detecting misclassified and out-of-distribution examples in neural networks. In *ICLR*, 2017. 6
- [35] Dan Hendrycks, Steven Basart, Mantas Mazeika, Mohammadreza Mostajabi, Jacob Steinhardt, and Dawn Song. A benchmark for anomaly segmentation. *arXiv preprint arXiv:1911.11132*, 2019. 2, 6
- [36] Dan Hendrycks, Steven Basart, Norman Mu, Saurav Kadavath, Frank Wang, Evan Dorundo, Rahul Desai, Tyler Zhu, Samyak Parajuli, Mike Guo, et al. Jacob steinhardt et justin gilmer. the many faces of robustness: A critical analysis of out-of-distribution generalization. In *ICCV*, 2021. 1
- [37] Dan Hendrycks, Nicholas Carlini, John Schulman, and Jacob Steinhardt. Unsolved problems in ml safety. *arXiv preprint arXiv:2109.13916*, 2021. 1
- [38] José Miguel Hernández-Lobato and Ryan Adams. Probabilistic backpropagation for scalable learning of bayesian neural networks. In *ICML*, 2015. 3
- [39] Stephen C Hora. Aleatory and epistemic uncertainty in probability elicitation with an example from hazardous waste management. *Reliability Engineering & System Safety*, 1996. 2
- [40] Jiri Hron, Roman Novak, Jeffrey Pennington, and Jascha Sohl-Dickstein. Wide bayesian neural networks have a simple weight posterior: theory and accelerated sampling. In *ICML*, pages 8926–8945. PMLR, 2022. 15
- [41] Eyke Hüllermeier and Willem Waegeman. Aleatoric and epistemic uncertainty in machine learning: An introduction to concepts and methods. *Machine Learning*, 2021. 2
- [42] Gabriel Ilharco, Mitchell Wortsman, Ross Wightman, Cade Gordon, Nicholas Carlini, Rohan Taori, Achal Dave, Vaishaal Shankar, Hongseok Namkoong, John Miller, Hananeh Hajishirzi, Ali Farhadi, and Ludwig Schmidt. Openclip, 2021. 3
- [43] Sergey Ioffe and Christian Szegedy. Batch normalization: Accelerating deep network training by reducing internal covariate shift. In *ICML*, 2015. 4
- [44] Pavel Izmailov, Sharad Vikram, Matthew D Hoffman, and Andrew Gordon Gordon Wilson. What are bayesian neural network posteriors really like? In *ICML*, 2021. 2, 4
- [45] Michael I Jordan, Zoubin Ghahramani, Tommi S Jaakkola, and Lawrence K Saul. An introduction to variational methods for graphical models. *ML*, 1999. 2
- [46] Alex Kendall and Yarin Gal. What uncertainties do we need in bayesian deep learning for computer vision? *NeurIPS*, 2017. 2
- [47] Alexander Kirillov, Eric Mintun, Nikhila Ravi, Hanzi Mao, Chloe Rolland, Laura Gustafson, Tete Xiao, Spencer Whitehead, Alexander C Berg, Wan-Yen Lo, et al. Segment anything. *arXiv preprint arXiv:2304.02643*, 2023. 3
- [48] Agustinus Kristiadi, Matthias Hein, and Philipp Hennig. Being bayesian, even just a bit, fixes overconfidence in relu networks. In *ICML*, 2020. 2
- [49] Alex Krizhevsky. Learning multiple layers of features from tiny images. Technical report, MIT, 2009. 1, 2, 6
- [50] A Krizhevsky, I Sutskever, and G Hinton. Imagenet classification with deep convolutional networks. In *NeurIPS*, 2012. 1
- [51] Balaji Lakshminarayanan, Alexander Pritzel, and Charles Blundell. Simple and scalable predictive uncertainty estimation using deep ensembles. In *NeurIPS*, 2017. 2, 3, 6, 8
- [52] John Lambert, Ozan Sener, and Silvio Savarese. Deep learning under privileged information using heteroscedastic dropout. In *CVPR*, pages 8886–8895, 2018. 17
- [53] Olivier Laurent, Emanuel Aldea, and Gianni Franchi. A symmetry-aware exploration of bayesian neural network posteriors. *arXiv preprint arXiv:2310.08287*, 2023. 4, 14
- [54] Olivier Laurent, Adrien Lafage, Enzo Tartaglione, Geoffrey Daniel, Jean-Marc Martinez, Andrei Bursuc, and Gianni Franchi. Packed-ensembles for efficient uncertainty estimation. In *ICLR*, 2023. 3
- [55] Kimin Lee, Kibok Lee, Honglak Lee, and Jinwoo Shin. A simple unified framework for detecting out-of-distribution samples and adversarial attacks. In *NeurIPS*, 2018. 2
- [56] Kaican Li, Kai Chen, Haoyu Wang, Lanqing Hong, Chaoqiang Ye, Jianhua Han, Yukuai Chen, Wei Zhang, Chunjing Xu, Dit-Yan Yeung, et al. Coda: A real-world road corner case dataset for object detection in autonomous driving. In *ECCV*, 2022. 1
- [57] Zhuang Liu, Hanzi Mao, Chao-Yuan Wu, Christoph Feichtenhofer, Trevor Darrell, and Saining Xie. A convnet for the 2020s. In *CVPR*, 2022. 4
- [58] David JC MacKay. A practical bayesian framework for backpropagation networks. *Neural computation*, 1992. 2, 3
- [59] Wesley J Maddox, Pavel Izmailov, Timur Garipov, Dmitry P Vetrov, and Andrew Gordon Wilson. A simple baseline for bayesian uncertainty in deep learning. In *NeurIPS*, 2019. 2
- [60] Andrey Malinin and Mark Gales. Predictive uncertainty estimation via prior networks. In *NeurIPS*, 2018. 2
- [61] Mahdi Pakdaman Naeini, Gregory F. Cooper, and Milos Hauskrecht. Obtaining well calibrated probabilities using bayesian binning. In *AAAI*, 2015. 6
- [62] Eric Thomas Nalisnick. *On priors for Bayesian neural networks*. University of California, Irvine, 2018. 2
- [63] Niv Nayman, Avram Golbert, Asaf Noy, Tan Ping, and Lih Zelnik-Manor. Diverse imagenet models transfer better. *arXiv preprint arXiv:2204.09134*, 2022. 2
- [64] Radford M Neal. *Bayesian learning for neural networks*. 2012. 2
- [65] Yuval Netzer, Tao Wang, Adam Coates, Alessandro Bischoff, Bo Wu, and Andrew Y. Ng. Reading digits in natural images with unsupervised feature learning. In *NeurIPS*, 2011. 6

- [66] Yannic Neuhaus, Maximilian Augustin, Valentyn Boreiko, and Matthias Hein. Spurious features everywhere-large-scale detection of harmful spurious features in imagenet. In *ICCV*, 2023. 1
- [67] Yaniv Ovadia, Emily Fertig, Jie Ren, Zachary Nado, David Sculley, Sebastian Nowozin, Joshua Dillon, Balaji Lakshminarayanan, and Jasper Snoek. Can you trust your model’s uncertainty? evaluating predictive uncertainty under dataset shift. In *NeurIPS*, 2019. 2
- [68] Adam Paszke, Sam Gross, Francisco Massa, Adam Lerer, James Bradbury, Gregory Chanan, Trevor Killeen, Zeming Lin, Natalia Gimelshein, Luca Antiga, et al. Pytorch: An imperative style, high-performance deep learning library. In *NeurIPS*, 2019. 6
- [69] Alec Radford, Karthik Narasimhan, Tim Salimans, Ilya Sutskever, et al. Improving language understanding by generative pre-training. Technical report, OpenAI, 2018. 1
- [70] Joseph Redmon, Santosh Divvala, Ross Girshick, and Ali Farhadi. You only look once: Unified, real-time object detection. In *CVPR*, 2016. 1
- [71] Tal Ridnik, Emanuel Ben-Baruch, Asaf Noy, and Lihi Zelnik-Manor. Imagenet-21k pretraining for the masses, 2021. 7
- [72] Hippolyt Ritter, Aleksandar Botev, and David Barber. A scalable laplace approximation for neural networks. In *ICLR*, 2018. 2, 3
- [73] Robin Rombach, Andreas Blattmann, Dominik Lorenz, Patrick Esser, and Björn Ommer. High-resolution image synthesis with latent diffusion models. In *CVPR*, 2022. 3
- [74] Subhankar Roy, Martin Trapp, Andrea Pilzer, Juho Kannala, Nicu Sebe, Elisa Ricci, and Arno Solin. Uncertainty-guided source-free domain adaptation. In *ECCV*, 2022. 3
- [75] Christoph Schuhmann, Romain Beaumont, Richard Vencu, Cade Gordon, Ross Wightman, Mehdi Cherti, Theo Coombes, Aarush Katta, Clayton Mullis, Mitchell Wortsman, et al. Laion-5b: An open large-scale dataset for training next generation image-text models. *NeurIPS*, 2022. 3
- [76] Aliaksei Severyn and Alessandro Moschitti. Learning to rank short text pairs with convolutional deep neural networks. In *SIGIR*, 2015. 1
- [77] Divya Shanmugam, Davis Blalock, Guha Balakrishnan, and John Guttag. Better aggregation in test-time augmentation. In *ICCV*, pages 1214–1223, 2021. 17
- [78] Jongwook Son and Seokho Kang. Efficient improvement of classification accuracy via selective test-time augmentation. *Information Sciences*, 642:119148, 2023. 17
- [79] Christian Szegedy, Vincent Vanhoucke, Sergey Ioffe, Jon Shlens, and Zbigniew Wojna. Rethinking the inception architecture for computer vision. In *CVPR*, 2016. 18
- [80] Luke Tierney and Joseph B Kadane. Accurate approximations for posterior moments and marginal densities. *Journal of the American Statistical Association*, 1986. 2, 3
- [81] Tishby, Levin, and Solla. Consistent inference of probabilities in layered networks: predictions and generalizations. In *IJCNN*, 1989. 2
- [82] Dustin Tran, Jeremiah Liu, Michael W Dusenberry, Du Phan, Mark Collier, Jie Ren, Kehang Han, Zi Wang, Zelda Mariet, Huiyi Hu, et al. Plex: Towards reliability using pretrained large model extensions. *arXiv preprint arXiv:2207.07411*, 2022. 1
- [83] Dmitry Ulyanov, Andrea Vedaldi, and Victor Lempitsky. Instance normalization: The missing ingredient for fast stylization. *arXiv preprint arXiv:1607.08022*, 2016. 4
- [84] Haoqi Wang, Zhizhong Li, Litong Feng, and Wayne Zhang. ViM: Out-of-distribution with virtual-logit matching. In *CVPR*, 2022. 6
- [85] Max Welling and Yee W Teh. Bayesian learning via stochastic gradient langevin dynamics. In *ICML*, 2011. 2
- [86] Yeming Wen, Dustin Tran, and Jimmy Ba. BatchEnsemble: an alternative approach to efficient ensemble and lifelong learning. In *ICLR*, 2019. 2, 3, 6
- [87] Ross Wightman. Pytorch image models. <https://github.com/rwightman/pytorch-image-models>, 2019. 18
- [88] Ross Wightman, Hugo Touvron, and Herve Jegou. Resnet strikes back: An improved training procedure in timm. In *NeurIPS*, 2021. 18
- [89] Andrew G Wilson and Pavel Izmailov. Bayesian deep learning and a probabilistic perspective of generalization. *NeurIPS*, 2020. 2, 4, 14
- [90] Guoxuan Xia and Christos-Savvas Bouganis. Window-based early-exit cascades for uncertainty estimation: When deep ensembles are more efficient than single models. In *ICCV*, 2023. 3
- [91] Fisher Yu, Haofeng Chen, Xin Wang, Wenqi Xian, Yingying Chen, Fangchen Liu, Vashisht Madhavan, and Trevor Darrell. Bdd100k: A diverse driving dataset for heterogeneous multitask learning. In *CVPR*, 2020. 6
- [92] Sangdoon Yun, Dongyoon Han, Seong Joon Oh, Sanghyuk Chun, Junsuk Choe, and Youngjoon Yoo. Cutmix: Regularization strategy to train strong classifiers with localizable features. In *CVPR*, 2019. 17
- [93] Éloi Zablocki, Hédi Ben-Younes, Patrick Pérez, and Matthieu Cord. Explainability of deep vision-based autonomous driving systems: Review and challenges. *IJCV*, 2022. 1
- [94] Sergey Zagoruyko and Nikos Komodakis. Wide residual networks. In *BMVC*, 2016. 1, 6
- [95] Xiaohua Zhai, Basil Mustafa, Alexander Kolesnikov, and Lucas Beyer. Sigmoid loss for language image pre-training. In *ICCV*, 2023. 3
- [96] Hongyi Zhang, Moustapha Cisse, Yann N Dauphin, and David Lopez-Paz. mixup: Beyond empirical risk minimization. In *ICLR*, 2018. 17

Make Me a BNN: A Simple Strategy for Estimating Bayesian Uncertainty from Pre-trained Models

Supplementary Material

Contents

A Theoretical Analysis	13
A.1. Stability of ABNN	13
A.2. Multi-modes with ABNN	14
A.3. Discussion on the Bayesian Neural Network Nature of ABNN	15
B Experiment on the variance of the gradient	15
C Discussion on stability of the training of ABNN	15
D Ablation study of ABNN and Sensitivity analysis	15
E Discussion on ABNN’s diversity	17
F. Extra Experiments	17
F.1. ViT transfer learning	17
F.2. Extra baselines	17
G Training hyperparameters	17
H Notations	18

The supplementary material encompasses multiple details and insights complementing the main paper as follows. In Section H, we introduce and clarify the notations used throughout the paper. Theoretical insights are presented in Section A, delving into the theoretical foundations of our methods. Section B evaluates the stability of ABNN, shedding light on its robustness. Section C shifts the focus to the stability of the training procedure, an essential aspect deserving exploration in every post-hoc technique. Section D delves into a sensitivity analysis and ablation study, exploring key components' resilience and performance impact. Section E focuses on the quality of the posterior estimated by ABNN. Finally, Sections G and F detail the training hyperparameters and showcase additional experiments, providing a comprehensive view of our methodology.

A. Theoretical Analysis

In this section, we develop a mathematical formalism to study the theoretical properties of ABNN.

A.1. Stability of ABNN

Variational inference BNNs [5] are not commonly used in computer vision due to their challenges in scaling properly for deeper high capacity DNNs [20]. In this section, we derive theoretical insights that entail the greater stability of ABNN, arguably also a Variational Inference BNN (VI-BNN). We start with deriving the gradients for a layer in a classic 2-hidden-layer MLP BNN. For the gradient of the loss on the mean of the weights of layer j , we have:

$$\frac{\partial \mathcal{L}_{\text{MAP}}(\boldsymbol{\omega})}{\partial W_{\mu, i, i'}^{(j)}} = \sum_{i''} \frac{\partial \mathcal{L}_{\text{MAP}}(\boldsymbol{\omega})}{\partial \mathbf{h}_{j+1, i''}} \left[W_{\mu, i'', i}^{(j+1)} + \mathcal{E}_{i'', i}^{(j+1)} W_{\sigma, i'', i}^{(j+1)} \right] \frac{a'(\mathbf{h}_{j, i}) \mathbf{a}_{j-1, i'}}{\sigma_j}. \quad (11)$$

On its standard deviation, we have:

$$\frac{\partial \mathcal{L}_{\text{MAP}}(\boldsymbol{\omega})}{\partial W_{\sigma, i, i'}^{(j)}} = \sum_{i''} \frac{\partial \mathcal{L}_{\text{MAP}}(\boldsymbol{\omega})}{\partial \mathbf{h}_{j+1, i''}} \left[W_{\mu, i'', i}^{(j+1)} + \mathcal{E}_{i'', i}^{(j+1)} W_{\sigma, i'', i}^{(j+1)} \right] \frac{a'(\mathbf{h}_{j, i}) \boldsymbol{\epsilon}_{j, i, i'} \mathbf{a}_{j-1, i'}}{\sigma_j}. \quad (12)$$

For the gradients of the ABNN parameters, in the case of a 2-hidden-layer MLP BNN, we have:

$$\frac{\partial \mathcal{L}_{\text{MAP}}(\boldsymbol{\omega})}{\partial \gamma_i^{(j)}} = \sum_{i''} \frac{\partial \mathcal{L}_{\text{MAP}}(\boldsymbol{\omega})}{\partial \mathbf{h}_{j+1, i''}} W_{i'', i}^{(j+1)} \frac{\mathbf{h}_j - \mu_j}{\sigma_j} (1 + \boldsymbol{\epsilon}_{j, i}) a'(\mathbf{u}_{j, i}), \quad (13)$$

as well as, on β ,

$$\frac{\partial \mathcal{L}_{\text{MAP}}(\boldsymbol{\omega})}{\partial \beta_{j, i}} = \sum_{i''} \frac{\partial \mathcal{L}_{\text{MAP}}(\boldsymbol{\omega})}{\partial \mathbf{h}_{j+1, i''}} W_{i'', i}^{(j+1)} a'(\mathbf{u}_{j, i}). \quad (14)$$

We have four random variables: $\frac{\partial \mathcal{L}_{\text{MAP}}(\boldsymbol{\omega})}{\partial \mathbf{h}_{j+1, i''}}$, $\mathcal{E}_{i'', i}^{(j+1)}$ and $\boldsymbol{\epsilon}_{j, i}$ along with $a'(\mathbf{u}_{j, i})$. Let's consider calculating the conditional variance given $\frac{\partial \mathcal{L}_{\text{MAP}}(\boldsymbol{\omega})}{\partial \mathbf{h}_{j+1, i''}}$ for all i'' . Assuming that all random variables associated with a single neuron are independent, we have:

$$\text{var} \left(\frac{\partial \mathcal{L}_{\text{MAP}}(\boldsymbol{\omega})}{\partial W_{\mu, i, i'}^{(j)}} \right) = \sum_{i''} \left(\frac{\partial \mathcal{L}_{\text{MAP}}(\boldsymbol{\omega})}{\partial \mathbf{h}_{j+1, i''}} \frac{W_{\sigma, i'', i}^{(j+1)} \mathbf{a}_{j-1, i'}}{\sigma_j} \right)^2 \times \text{var} \left[\mathcal{E}_{i'', i}^{(j+1)} a'(\mathbf{h}_{j, i}) \right] \quad (15)$$

and

$$\text{var} \left(\frac{\partial \mathcal{L}_{\text{MAP}}(\boldsymbol{\omega})}{\partial W_{\sigma, i, i'}^{(j)}} \right) = \sum_{i''} \left(\frac{\partial \mathcal{L}_{\text{MAP}}(\boldsymbol{\omega})}{\partial \mathbf{h}_{j+1, i''}} \frac{W_{\sigma, i'', i}^{(j+1)} \mathbf{a}_{j-1, i'}}{\sigma_j} \right)^2 \text{var} \left[\mathcal{E}_{i'', i}^{(j+1)} a'(\mathbf{h}_{j, i}) \boldsymbol{\epsilon}_{j, i, i'} \right]. \quad (16)$$

Using the fact that $\boldsymbol{\epsilon}_{j, i, i'}$ is independent of $\mathcal{E}_{i'', i}^{(j+1)}$ and $a'(\mathbf{h}_{j, i})$ we have that

$$\text{var} \left[\mathcal{E}_{i'', i}^{(j+1)} a'(\mathbf{h}_{j, i}) \boldsymbol{\epsilon}_{j, i, i'} \right] = \text{var} \left[\mathcal{E}_{i'', i}^{(j+1)} a'(\mathbf{h}_{j, i}) \right] + \mathbb{E} \left(\mathcal{E}_{i'', i}^{(j+1)} a'(\mathbf{h}_{j, i}) \right)^2 \quad (17)$$

In the case of ABNN, we can express the conditional variance as follows:

$$\text{var} \left(\frac{\partial \mathcal{L}_{\text{MAP}}(\boldsymbol{\omega})}{\partial \gamma_i^{(j)}} \right) = \sum_{i''} \left(\frac{\partial \mathcal{L}_{\text{MAP}}(\boldsymbol{\omega})}{\partial \mathbf{h}_{j+1, i''}} W_{i'', i}^{(j+1)} \frac{\mathbf{h}_j - \mu_{\mathbf{h}_j}}{\sigma_j} \right)^2 \text{var} \left[\boldsymbol{\epsilon}_{j, i} a'(\mathbf{u}_{j, i}) \right] \quad (18)$$

$$\text{var} \left(\frac{\partial \mathcal{L}_{\text{MAP}}(\boldsymbol{\omega})}{\partial \beta_{j, i}} \right) = \sum_{i''} \left(\frac{\partial \mathcal{L}_{\text{MAP}}(\boldsymbol{\omega})}{\partial \mathbf{h}_{j+1, i''}} W_{i'', i}^{(j+1)} \right)^2 \text{var} \left[a'(\mathbf{u}_{j, i}) \right] \quad (19)$$

Assuming that $\text{var} \left[\boldsymbol{\epsilon}_{j, i} a'(\mathbf{u}_{j, i}) \right] = \text{var} \left[\mathcal{E}_{i'', i}^{(j+1)} a'(\mathbf{h}_{j, i}) \right]$,

we find that the variances of $\text{var} \left(\frac{\partial \mathcal{L}_{\text{MAP}}(\boldsymbol{\omega})}{\partial W_{\mu, i, i'}^{(j)}} \right)$ and $\text{var} \left(\frac{\partial \mathcal{L}_{\text{MAP}}(\boldsymbol{\omega})}{\partial W_{\sigma, i, i'}^{(j)}} \right)$ are directly proportional to the variance of $\text{var} \left(\frac{\partial \mathcal{L}_{\text{MAP}}(\boldsymbol{\omega})}{\partial \gamma_{j, i}} \right)$. This proportionality is associated with the magnitudes of the weight values, and we assume that they are of similar magnitude. Consequently, the variance of the gradient of the parameters $\beta_{j, i}$ is the smallest among all, followed by the variance of the parameters $\gamma_{j, i}$ and $W_{\mu, i, i'}^{(j)}$, which are roughly equivalent, with the highest variance observed for $W_{\sigma, i, i'}^{(j)}$. This property results in more stable backpropagation for ABNN compared to classic VI-BNNs.

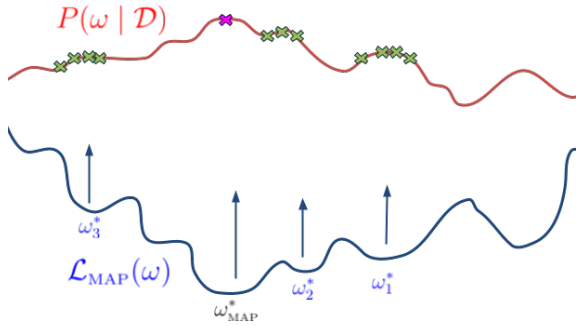


Figure 4. Illustration of the training loss (in blue) and the corresponding posterior distribution (in red). Due to the multi-modal nature of the posterior, training multiple ABNNs with distinct final weights (such as ω_1^* , ω_2^* , and ω_3^*) enables sampling from different modes, enhancing the overall estimation of the posterior.

A.2. Multi-modes with ABNN

The posterior of the DNN often comprises multiple modes [53, 89], making it non-trivial for a unimodal distribution chosen to represent the BNN’s posterior to account for these different modes effectively. One approach to address this issue is to train multiple BNNs, as proposed in the multi-SWAG method by Wilson and Izmailov [89]. However, adapting this strategy to VI-BNNs inherits the instability issue from classic BNNs and may struggle to fit multiple modes accurately.

Our solution, ABNN, also faces a similar challenge, where we need to ensure that the technique doesn’t collapse into the same local minima during training. We introduce a small perturbation to the loss function to prevent this collapse, which helps diversify the optimization process. This perturbation involves modifying the class weights within the cross-entropy loss. More precisely, contrary to classic VI-BNN that optimizes the Evidence Lower Bound (ELBO) loss, we propose to maximize the MAP. ABNNs optimize the following loss:

$$\mathcal{L}(\omega) = - \sum_{(\mathbf{x}_i, y_i) \in \mathcal{D}} \alpha(y_i) \log P(y_i | \mathbf{x}_i, \omega) - \log P(\omega), \quad (20)$$

In the standard cross-entropy loss, all classes are given equal weight, typically represented as $\alpha(y_i) = 1$. However, our approach deliberately introduces the *random prior*: random weight adjustments for certain classes, denoted as η_i (such that $\alpha(y_i) = 1 + \eta_i$). This manipulation encourages various ABNNs to specialize as experts in different classes. Consequently, the training loss is formulated as follows:

$$\mathcal{L}(\omega) = \mathcal{L}_{\text{MAP}}(\omega) + \mathcal{E}(\omega) \quad (21)$$

where

$$\mathcal{E}(\omega) = - \sum_{(\mathbf{x}_i, y_i) \in \mathcal{D}} \eta_i \log P(y_i | \mathbf{x}_i, \omega). \quad (22)$$

Let’s denote $\omega^{(0)}$ as the parameter configuration that minimizes \mathcal{L}_{MAP} . Let us suppose for simplicity that the loss function is convex to provide a theoretical grounding to the random prior. After a single step of gradient descent (GD), we have:

$$\omega^{(1)} = \omega^{(0)} - \lambda \nabla \mathcal{L}(\omega^{(0)}), \quad (23)$$

where $\omega^{(1)}$ represents the parameters after the first optimization step, the superscript denotes the iteration number, and λ is the learning rate.

We can express the updated loss $\mathcal{L}(\omega^{(1)})$ using the GD, as shown in Eq. (24):

$$\mathcal{L}(\omega^{(1)}) = \mathcal{L}(\omega^{(0)} - \lambda \nabla \mathcal{L}(\omega^{(0)})) \quad (24)$$

Now, by applying a first-order Taylor expansion to \mathcal{L} , we can express the updated loss $\mathcal{L}(\omega^{(1)})$ as a function of the initial loss $\mathcal{L}(\omega^{(0)})$ and the gradient update, as shown in Eq. (25):

$$\mathcal{L}(\omega^{(1)}) = \mathcal{L}(\omega^{(0)}) - \lambda \nabla \mathcal{L}(\omega^{(0)})^t \nabla \mathcal{L}(\omega^{(0)}) \quad (25)$$

This equation can be further simplified by noticing that $\nabla \mathcal{L}_{\text{MAP}}(\omega^{(0)}) = 0$:

$$\mathcal{L}(\omega^{(1)}) = \mathcal{L}(\omega^{(0)}) - \lambda \nabla \mathcal{E}(\omega^{(0)})^t \nabla \mathcal{E}(\omega^{(0)}) \quad (26)$$

Starting with Eq. (26), we have:

$$\begin{aligned} \mathcal{L}(\omega^{(1)}) = \mathcal{L}(\omega^{(0)}) - \lambda \sum_{(\mathbf{x}_i, y_i) \in \mathcal{D}} \sum_{(\mathbf{x}_{i'}, y_{i'}) \in \mathcal{D}} \eta_i \eta_{i'} \\ \log P(y_{i'} | \mathbf{x}_{i'}, \omega^{(0)}) \log P(y_i | \mathbf{x}_i, \omega^{(0)}) \end{aligned} \quad (27)$$

Under the assumption that $\lambda \eta_i \eta_{i'}$ is small and that $\log P(y_{i'} | \mathbf{x}_{i'}, \omega)$ is bounded, we can approximate the loss as follows: $\mathcal{L}(\omega^{(1)}) \simeq \mathcal{L}(\omega^{(0)})$. Consequently, we have $\nabla \mathcal{L}(\omega^{(1)}) \simeq \nabla \mathcal{L}(\omega^{(0)})$, and after another optimization step, $\omega^{(2)}$ is updated as $\omega^{(2)} = \omega^{(1)} - \lambda \nabla \mathcal{L}(\omega^{(1)}) = \omega^{(0)} - 2\lambda \nabla \mathcal{L}(\omega^{(0)})$.

By applying the same technique iteratively, for all t , we can approximate the loss as $\mathcal{L}(\omega^{(t)}) \simeq \mathcal{L}(\omega^{(0)})$. This leads also to the relationship $\omega^{(t)} = \omega^{(0)} - t\lambda \nabla \mathcal{L}(\omega^{(0)})$.

Under the conditions that the loss is convex, the derivatives of the DNN are bounded, and $\lambda \eta_i \eta_{i'}$ is small, we can find minima of \mathcal{L} with similar loss values by introducing weight diversity. This loss function can be valuable in encouraging each DNN to escape from the global minima, particularly in convex cases. In non-convex cases, standard SGD may already help escape from local minima, but this additional loss may offer extra assistance in avoiding the same local minima. In Figure 4, we present a visualization

depicting the training loss alongside the posterior distribution. This Figure highlights the importance of training multiple ABNNs with different optimal solutions to improve the quality in estimating the posterior distribution.

A.3. Discussion on the Bayesian Neural Network Nature of ABNN

The Law of the Unconscious Statistician (LOTUS) [21] is a theorem in probability theory that offers a method for computing the expected value of a function of a random variable. Hence, for a continuous random variable X with a probability density function $f_X(x)$, the expected value of a function $Y = g(X)$ is expressed as:

$$E_Y(Y) = E_X[g(X)] \quad (28)$$

In our scenario, let U_j denote the random variable associated with \mathbf{u}_j , and $W^{(j)}$ represent the random variable $W^{(j)}$ (we use the same letter for simplification). Thus, we have:

$$E_{U_j}(U_j) = \frac{\mathbf{h}_j - \mu_{\mathbf{h}_j}}{\sqrt{\sigma_{\mathbf{h}_j}^2 + \epsilon}} \gamma_j + \beta_j \quad (29)$$

For simplification, we set $\beta_j=0$, which leads to

$$\text{var}_{U_j}(U_j) = \left(\frac{\mathbf{h}_j - \mu_{\mathbf{h}_j}}{\sqrt{\sigma_{\mathbf{h}_j}^2 + \epsilon}} \gamma_j \right)^2 \quad (30)$$

Here, the parameters γ_j and β_j are optimized to obtain the best Bayesian Neural Network (BNN)

B. Experiment on the variance of the gradient

To validate our hypothesis that ABNN is more stable than VI-BNNs, as detailed in section A.1, we analyze the variances of the gradients of classic DNNs, VI-BNNs, and ABNNs. Table 4 reveals that the gradient variance of BNNs are significantly greater than that of DNNs, aligning with the inherent challenges in training BNNs. Notably, ABNN exhibits a considerably lower gradient, stemming from only the weights of BNL are trained. Both empirical observations and theoretical considerations affirm the superior stability of ABNN on this side. Additionally, Table 4 includes results for a VI-BNN, which, as discussed in this section, exhibits suboptimal performance. Noteworthy other works [20, 40] also express concerns regarding the stability of VI-BNNs.

C. Discussion on stability of the training of ABNN

ABNN being a post-hoc technique, it is imperative to ensure that it does not introduce instability to DNNs, especially in the critical domain of uncertainty quantification.

Method	variance (10^{-4})
ResNet50	1.43
ResNet50 BNN	2.54
ResNet50 ABNN	$3.20 \cdot 10^{-2}$
Wide-ResNet	1.37
Wide-ResNet BNN	2.53
Wide-ResNet ABNN	$9.91 \cdot 10^{-2}$

Table 4. **Variance of gradients on relevant parameters**

Single model: every weight (no bias)

BNN: means of the weight samplers

ABNN: parameters linked to the BNL layers

	Acc	ECE	AUPR	AUC	FPR95
Single model	0.356	0.0002	1.036	1.445	2.740
one ω_{MAP} + Multiple ABNN	0.066	0.0009	0.130	0.224	0.658
Multiple ω_{MAP} + ABNN	0.324	0.0011	1.131	1.570	3.202

Table 5. **Standard Deviation (SD) Comparison of ABNN and DNN.**

The first row presents the SD of a single DNN, while the second row depicts the SD of ABNN starting from a single checkpoint. The last row quantifies the SD of ABNN when trained from different checkpoints. All training scenarios use the optimal hyperparameters for ABNN on a ResNet-50 architecture on the CIFAR-10 dataset.

We train multiple single models based on a ResNet-50 architecture on CIFAR-10 to verify this point, calculating the standard deviation of the different metrics. Additionally, we derive several ABNNs starting from these checkpoints and assess the variance. Finally, we apply our technique to train an ABNN for each checkpoint of the single models. Table 5 demonstrates that our approach minimally increases the variance, confirming that it does not introduce instability to the uncertainty quantification process.

D. Ablation study of ABNN and Sensitivity analysis

In Table 6, we conduct a study to inspect the impact of adding or removing two characteristics from our method. First, we investigate whether the addition of the random prior (linked to \mathcal{E} term in Eq. (22)), which introduces disturbance to the loss, improves the performance of ABNN. We test the Random Prior (RP) to check whether \mathcal{E} contributes positively. Notably, when training a single RP model (when **MM** is \times), it appears to degrade performance as it corrupts the cross-entropy. Conversely, in the case of training multiple ABNNs (**MM** is \checkmark), RP seems to improve uncertainty quantification metrics. The second aspect is the training of multiple modes: Table 6 shows that incorporating multiple modes (**MM** is \checkmark) improves the quality of the uncertainty quantification, in particular for OOD detection.

		RP	MM	Acc \uparrow	ECE \downarrow	AUPR \uparrow	AUC \uparrow	FPR95 \downarrow
CIFAR-10	ResNet-50	\times	\times	94.7	1.0	96.8	94.1	17.3
		\checkmark	\times	95.2	0.89	96.7	94.4	15.3
		\times	\checkmark	95.3	1.34	97.1	94.8	15.7
		\checkmark	\checkmark	95.4	0.845	97.0	94.7	15.1
	WideResNet	\times	\times	94.4	1.34	96.4	93.7	18.2
		\checkmark	\times	92.8	2.2	97.5	95.3	14.8
		\times	\checkmark	94.9	1.38	97.3	95.1	15.7
		\checkmark	\checkmark	93.7	1.8	98.5	96.9	12.6
CIFAR-100	ResNet-50	\times	\times	78.8	5.7	89.3	80.8	50.4
		\checkmark	\times	78.7	5.5	89.4	81.0	50.1
		\times	\checkmark	78.3	5.8	89.6	81.6	48.2
		\checkmark	\checkmark	78.8	5.6	89.7	81.6	49.0
	WideResNet	\times	\times	80.5	5.6	84.0	72.6	62.2
		\checkmark	\times	79.6	5.5	84.7	74.9	55.8
		\times	\checkmark	80.4	5.5	85.0	75.0	57.7
		\checkmark	\checkmark	78.2	5.9	87.8	79.7	49.0

Table 6. Performance comparison (averaged over five runs) on CIFAR-10/100 using ResNet-50 and WideResNet28 \times 10. RP is Random Prior, and MM is multi-mode. For OOD detection, we use the SVHN dataset.

Coef. LR	Acc \uparrow	ECE \downarrow	AUPR \uparrow	AUC \uparrow	FPR95 \downarrow
$\times 10^{-1}$	95.5	0.9	96.2	93.0	20.7
$\times 2 \cdot 10^{-1}$	95.4	0.9	96.5	93.8	18.2
$\times 5 \cdot 10^{-1}$	95.4	1.0	96.3	93.3	19.9
$\times 1$	95.4	0.9	97.0	94.7	15.1
$\times 2$	95.3	1.1	95.7	92.3	22.0
$\times 5$	94.6	1.5	96.1	93.1	19.6
$\times 10$	93.9	1.1	96.7	94.2	19.2

Table 7. Sensitivity Analysis of the Learning Rate on CIFAR-10. e conducted training for ABNN using a learning rate set at 0.0057 multiplied by the Coef LR.

Coef. LR	Acc \uparrow	ECE \downarrow	AUPR \uparrow	AUC \uparrow	FPR95 \downarrow
$\times 10^{-1}$	79.0	5.4	89.0	80.3	51.5
$\times 2 \cdot 10^{-1}$	78.9	5.5	88.6	79.9	52.5
$\times 5 \cdot 10^{-1}$	78.9	5.6	88.9	80.0	52.5
$\times 1$	78.9	5.5	89.4	81.0	50.1
$\times 2$	78.8	5.7	88.6	79.8	52.6
$\times 15$	79.0	5.5	88.8	80.1	52.0
$\times 10$	78.8	5.7	88.8	80.2	51.4

Table 8. Sensitivity Analysis of the Learning Rate on CIFAR-100. e conducted training for ABNN using a learning rate set at 0.00139 multiplied by the Coef. LR.

We analyze the performance variations in Tables 7 and 8 by modifying the learning rate during the fine-tuning phase. It’s essential to highlight that this hyperparameter is the only

one of ABNN. We fine-tune a single model with various learning rates for this evaluation after adapting it to ABNN. Remarkably, the learning rate appears non-critical, as the performances on CIFAR-10 and CIFAR-100 exhibit minimal variations, around one percent.

E. Discussion on ABNN’s diversity

We trained a Deep Ensembles of ResNet-50 architecture for 200 epochs, specifically three networks. As demonstrated in [22], Deep Ensembles strikes a good balance between accuracy and diversity, enabling effective uncertainty quantification. Simultaneously, we train three ABNNs, initializing them from the same checkpoint. It’s important to highlight that all ABNN parameters were trained for this experiment. To visually compare the results, akin to [22] (Figure 2.c), we conduct a t-SNE analysis on the latent space of all the checkpoints after each epoch. Initially, ABNN shows limited diversity due to having only one checkpoint. However, as training progresses, some diversity emerges, though less than observed in Deep Ensembles. Table 9 illustrates that ABNN exhibits lower mutual information than BNN on both in-distribution (IDs) and out-of-distribution (OOD) samples. Yet, interestingly, ABNN achieves a superior mutual information ratio on OODs/IDs. It’s worth noting that mutual information serves as a metric for measuring diversity and can also quantify epistemic uncertainty. Mutual information is defined for a finite set $\{\omega_1, \dots, \omega_M\}$ of M weight configurations sampled from the posterior distribution as :

$$\underbrace{I(P(\omega | \mathcal{D}))}_{\text{Epistemic uncertainty}} = \underbrace{\mathcal{H}\left(\frac{1}{M} \sum_{m=1}^M P(y | \mathbf{x}, \omega_m)\right)}_{\text{Total uncertainty}} - \underbrace{\frac{1}{M} \sum_{m=1}^M \mathcal{H}(P(y | \mathbf{x}, \omega_m))}_{\text{Aleatoric uncertainty}}. \quad (31)$$

with $\mathcal{H}(\cdot)$ the entropy is defined by :

$$\mathcal{H}(P(y | \mathbf{x}, \omega)) = - \sum_y P(y_i | \mathbf{x}_i, \omega) \log P(y_i | \mathbf{x}_i, \omega) \quad (32)$$

The good mutual information ratio highlights ABNN’s superior ability to detect out-of-distribution samples compared to BNN. Moreover, Figure 3 illustrates that benefiting from multiple training instances, ABNN can effectively model multi-modes—a capability beyond the reach of classical BNNs. This is particularly valuable given the inherent multi-modal nature of the posterior.

F. Extra Experiments

F.1. ViT transfer learning

We also show that ABNN can be used in contexts of transfer learning. Table 10 presents the comparative performance of ViT B-16 pre-trained on ImageNet-21k and fine-tuned with

	ID	OOD	OOD/ID
ABNN	1.39e-4	5.22e-4	3.76
BNN	0.139	0.179	1.28

Table 9. **Evaluation of the average Mutual Information** on the test set and the OOD set of the different sample from an ABNN or a BNN.

and without a mono-modal ABNN on CIFAR-100 in 10,000 steps. Despite the mono-modality of ABNN in this experiment, we show that the corresponding ViT outperforms the classic fine-tuning in calibration and AUPR.

	Acc	ECE	AUPR	AUC	FPR95
Single model	92.0	4.4	96.6	92.7	28.1
ABNN	91.9	1.4	96.9	92.5	33.9

Table 10. **Transfer learning of a ViT pre-trained on ImageNet-21k on CIFAR-100.** The first line is the classic pre-trained model fine-tuned with ABNN, and the second is fine-tuned with the classic layer normalization.

F.2. Extra baselines

To benchmark our method against other posthoc techniques, we implement a variant of Test-Time Augmentation [2, 77, 78], incorporating random Gaussian noise with a specified standard deviation of 0.08. The objective is to introduce diversity and ensemble different predictions by leveraging the added noise. Like [52], we experimented with adding noise to the latent space, representing the scenario where ABNN is not trained. We tested various levels of standard deviation, and the corresponding results are summarized in Table 11. Notably, the untrained ABNN does not perform effectively, underscoring the significance of a brief finetuning phase. Additionally, we train a VI-BNN, a non-posthoc technique, to understand the performance of a traditional BNN. It’s noteworthy that VI-BNNs proved challenging to train and demonstrated subpar performance.

G. Training hyperparameters

Table 12 provides a detailed overview of all the hyperparameters employed throughout our study. We use SGD in conjunction with a multistep learning-rate scheduler for image classification tasks, adjusting the rate by multiplying it by γ -lr at each milestone. It’s important to note that, for stability reasons, BatchEnsemble based on ResNet-50 employed a lower learning rate of 0.08, deviating from the default 0.1. Our "Medium" data augmentation strategy encompasses a blend of Mixup [96] and Cutmix [92], with a

	Acc \uparrow	ECE \downarrow	AUPR \uparrow	AUC \uparrow	FPR95 \downarrow	
CIFAR-10	Single model	95.53	0.83	96.52	93.70	18.43
	VI BNN	75.66	5.40	80.60	69.53	66.62
	Test-Time Augmentation	89.95	2.49	93.78	89.95	25.12
	Noise on latent space std=0.01	95.51	0.82	96.51	93.68	18.56
	Noise on latent space std=0.1	95.46	0.90	95.88	92.64	20.94
	Noise on latent space std=1	18.66	31.58	71.89	50.86	93.27
	ABNN	95.43	0.85	97.03	94.73	15.11
CIFAR-100	Single model	79.05	5.34	88.72	79.96	52.04
	VI BNN	41.17	8.97	78.44	61.82	86.15
	Test-Time Augmentation	72.65	7.67	86.64	76.89	55.52
	Noise on latent space std=0.01	79.03	5.39	88.68	79.85	52.54
	Noise on latent space std=0.1	77.49	6.36	86.53	75.19	64.42
	Noise on latent space std=1	01.03	11.91	74.08	50.92	95.74
	ABNN	78.94	5.47	89.36	81.04	50.12

Table 11. Performance comparison of different Post-hoc and BNN uncertainty quantification baselines on CIFAR-10/100 using ResNet-50.

switch probability of 0.5. Additionally, `timm`'s augmentation classes [87] were incorporated with coefficients of 0.5 and 0.2. RandAugment [11] with parameters $m = 9$, $n = 2$, and $mstd = 1$, along with label-smoothing [79] of intensity 0.1, were also applied.

In the case of ImageNet, we follow the A3 procedure outlined in [88] for all models. It's worth mentioning that training according to the exact A3 procedure was not consistently feasible; please refer to the specific subsections for additional details.

We highlight that, to enhance training stability and fasten the training, we introduce a hyperparameter α in the BNL layer. This transforms the layer as follows:

$$\mathbf{BNL}(\mathbf{h}_j) = \frac{\mathbf{h}_j - \hat{\mu}_j}{\hat{\sigma}_j} \times \gamma_j(1 + \epsilon_j\alpha) + \beta_j. \quad (33)$$

$$(34)$$

The hyperparameter α is typically set to 0.01, except in the case of ViT, where specific considerations may apply.

H. Notations

We summarize the main notations used in the paper in Table 14.

Dataset	Networks	Epochs	Batch size	start lr	Momentum	Weight decay	γ -lr	Milestones	Data augmentations
C10	R50	200	128	0.1	0.9	$5 \cdot 10^{-4}$	0.2	60, 120, 160	HFlip
C10	WR28-10	200	128	0.1	0.9	$5 \cdot 10^{-4}$	0.2	60, 120, 160	HFlip
C100	R50	200	128	0.1	0.9	$5 \cdot 10^{-4}$	0.2	60, 120, 160	HFlip
C100	WR28-10	200	128	0.1	0.9	$5 \cdot 10^{-4}$	0.2	60, 120, 160	Medium

Table 12. **Hyperparameters for image classification experiments.** HFlip denotes the classical horizontal flip.

Dataset	Networks	Epochs	Batch size	start lr	Alpha	Momentum	Weight decay	γ -lr	Milestones	Data augmentations
C10	R50	2	128	0.0057	0.01	0.9	$5 \cdot 10^{-4}$	/	/	HFlip
C10	WR28-10	2	128	0.0091	0.01	0.9	$5 \cdot 10^{-4}$	/	/	HFlip
C100	R50	10	128	0.00139	0.01	0.9	$5 \cdot 10^{-4}$	0.5	5	HFlip
C100	WR28-10	10	128	0.034	0.01	0.9	$5 \cdot 10^{-4}$	0.5	5	HFlip
Imagenet	R50	1	128	0.00439	0.01	0.9	$5 \cdot 10^{-4}$	/	/	HFlip
Imagenet	ViT	0.25	128	$7.33 \cdot 10^{-6}$	0.00035	0.9	$7 \cdot 10^{-6}$	$5 \cdot 10^{-4}$	Constant	HFlip
StreetHazards	DeepLabv3+	10	4	0.01	0.01	0.9	$1 \cdot 10^{-4}$	0.9	Polynomial	HFlip, RandomCrop, ColorJitter, RandomScale
BDD-Anomaly	DeepLabv3+	10	4	0.01	0.01	0.9	$1 \cdot 10^{-4}$	0.9	/	HFlip, RandomCrop, ColorJitter, RandomScale
MUAD	DeepLabv3+	6	4	0.044	0.01	0.9	$1 \cdot 10^{-4}$	0.9	/	HFlip, RandomCrop, ColorJitter, RandomScale

Table 13. **Hyperparameters for image classification experiments with ABNN.** HFlip denotes the classical horizontal flip. Random prior has been used.

Table 14. **Summary of the main notations of the paper.**

Notations	Meaning
$\mathcal{D} = \{(\mathbf{x}_i, \mathbf{y}_i)\}_{i=1}^N$	The set of N data samples and the corresponding labels
j	The index of the current layer
ω	The set of all the weights of the DNN
$\omega_m \sim P(\omega \mathcal{D})$	The m -th sample from the concatenation of weights of the posterior of the DNN.
M	The number of networks in an ensemble
$\omega^{(t)}$	The concatenation of all the weights of the DNN after t steps of optimization
\mathbf{h}_j	The pre-activation feature map and output of layer $(j - 1)$ & input of layer j before normalization
\mathbf{u}_j	The pre-activation feature map and output of layer $(j - 1)$ & input of layer j before normalization
$\gamma_j \beta_j$	The parameters of the batch, instance, or layer normalization of layer j
$\mu_j \sigma_j$	The empirical mean and variance used by the batch, instance, or layer normalization of layer j
\mathbf{a}_j	The feature map and output of layer j , $\mathbf{a}_j = a(\mathbf{u}_j)$
$a(\cdot)$	The activation function
$W^{(j)}$	The weights of the j -th layer in a Multi-Layer Perceptron (MLP).
$W_\mu^{(j)}$	The mean weights of the j -th layer in a BNN MLP
$W_\sigma^{(j)}$	The standard variation weights of the j -th layer in a BNN MLP
$\epsilon^{(j)} \sim \mathcal{N}(\mathbf{0}, \mathbb{1})$	A vector sampled from a standard normal distribution at layer j
ϵ	The concatenation of all the j - the $\epsilon^{(j)}$ of each layer j
ϵ_l	The l -th sample of ϵ
\mathcal{H}	The entropy function